Journal of Visualization, Vol. 5, No. 4 (2002) 371-379

A Study on Generation of Noise by High-Speed Pulsating Jets

Kimura, A.* and Iwamoto, J.*

* Department of Mechanical Engineering, Tokyo Denki University, 2-2 Kanda-Nishiki-cho, Chiyoda-ku, Tokyo 101-8457, Japan.

Received 15 February 2002.
Revised 31 March 2002.

***Abstract*:** This paper describes the noise generation in an exhaust system of a reciprocating engine and focuses on the noise generated by shock/vortex interaction. The pulsating flow through the exhaust pipe consists of the compression and expansion wave, shock wave being generated by the non-linearity of the compression wave at its head. The jet noise is produced when the pulsating flow is discharged from the pipe end into atmosphere. The numerical simulation based on a finite difference method and experiment were made, the result of both of them being compared. First, the flow field in the pipe was obtained to easily discuss the characteristic of the pulsating jet in terms of the pressure history in the pipe. The jet structure was visualized by using schlieren and shadowgraph techniques. Sound pressure measurements at various locations were made in order to survey the directivity of the noise. The comparison between the result of numerical calculation and experiment showed a good agreement. A noise source related to shock/vortex interaction was confirmed by the numerical study clearly.

***Keywords*:** compressible flow, pulsating jet, shock/vortex interaction, noise generation.

1. Introduction

Reciprocating engine has been used in many industrial applications such as automobile, airplane, vessel, and so on. Automobile is a representative of these. It is well-known that flow through the exhaust pipe of a reciprocating engine is high-speed and pulsating. Periodic opening and shutting of the exhaust valve produce the flow pulsation in the exhaust pipe. It has been concluded by many studies (Blair and Goulburn, 1967; Blair and Arbuckle, 1970) that shock wave is formed as compression wave generated by opening of the valve propagates downstream along the pipe. The shock wave becomes dominant noise source when it is discharged into atmosphere. However, Endo and Iwamoto (1999) pointed out the existence of another noise which appears in the flow field behind the discharged shock wave. In their numerical study, Yee's symmetric type TVD scheme (Yee, 1989) was used. Unfortunately their results did not clarify the process of generation of the noise since the numerical scheme did not have enough resolution to capture sound waves because of low accuracy.

In the present study, our goal is to obtain a detailed information of the flow field and to clarify how the noise of pulsating jet is emitted. In the experimental study, shadowgraph and schlieren methods are applied to visualize the flow field. In numerical study, we assumed that flow field in the exhaust pipe should be one-dimensional and the calculation using a TVD scheme was conducted by solving 1-D Euler equation. As mentioned above, the most important thing for capturing sound wave is a high accuracy of a scheme applied to the spatial domain. Hence, we employed fifth-order TVD scheme to investigate pulsating jet numerically.

2. Experimental Apparatus

A schematic view of an experimental apparatus is shown in Fig. 1. Compressed air from two compressors passed through an air-dryer, a surge tank and an oil mist separator, is being steadily supplied into the high-pressure chamber shown in Fig. 1. The air stored in the high-pressure chamber flows into a pipe after passing through a rotary valve (Iwamoto, 1974) which can generate the pulsating flow. Pulsating flow through the pipe is discharged from the pipe end into a soundproof room which is under atmospheric condition. The pipe is straight and 1 m long, the inner diameter being 13 mm. The rotary disk has two ports placed symmetrically with respect to the central point of the rotary disk and the area change is designed to be equal to that of an exhaust port of a typical four cycle internal combustion engine. The volume of the soundproof room, into which the pulsating jet is discharged, is large enough (W: 2400 mm D: 2800 mm H: 2100 mm), so that the pressure rise can be neglected.

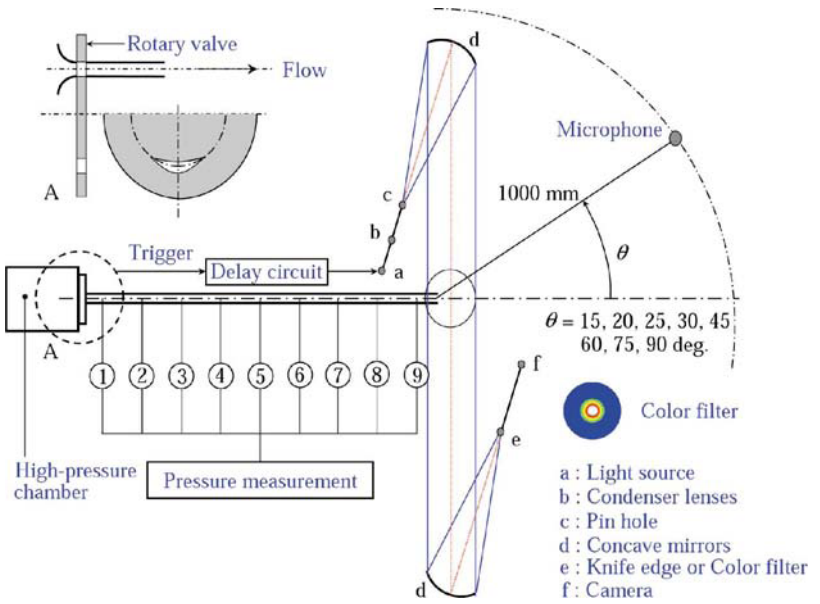

Fig. 1. Schematic view of experimental apparatus.

Nine stations are located along the pipe for measuring pressure histories via static pressure holes using pressure transducers of a semi-conductor type. The primary resonant frequency of the transducers is 40 kHz. The measurement begins (t = 0 sec) at the moment when the rotary valve starts to open and the synchronized signal is also used for flow visualization. The distance between neighboring pressure holes is 100 mm. The pressure in the high-pressure chamber is kept at 4.0 atm, which is almost equal to the pressure in cylinders of a typical four cycle engine at the moment when the exhaust valve begins to open. In the soundproof room, visualization of the flow field near the pipe end using schlieren, color schlieren and shadowgraph techniques can be made. Color schlieren technique is suitable for observing the change in density of the whole flow field because it is easy to sensitively distinguish the change of color rather than that of hue of black and white. The visualization system illustrated in Fig. 1 employs a Xenon discharge tube of 180 nsec flash source. The timing of light can be adjusted by a delay unit into which the synchronized signal mentioned above is sent. The synchronized signal associated with the revolution of the rotary valve is output in succession and those signals are used for visualization as mentioned above, whereby the photographs can be taken at different timings by using the signals at different periods of the rotary valve. In addition, it should be noted that the speed of the rotary valve is controlled in error by less than 0.1%. Sound pressure measurement is made with an electrostatic microphone which is set at different locations shown in Fig. 1. In the experiment, the speed of the rotary valve corresponding to 6000 rpm of a real engine is fixed, which generates typical flow field with shock wave present.

3. Numerical Method

In the numerical simulation, there are two computational domains which are solved separately. One is the flow field between the entrance to the pipe at the rotary valve and the downstream end of the pipe, flow in the pipe being assumed to be one-dimensional, frictionless and adiabatic. The governing equation is given by,

$$\frac{\partial \boldsymbol{U}}{\partial t} + \frac{\partial \boldsymbol{F}}{\partial x} = 0 \tag{1}$$

where t is the time, x the distance along the pipe, $\boldsymbol{U} = [\ \rho\ \rho u\ e\ ]^T$ and $\boldsymbol{F} = [\ \rho u\ p + \rho u^2\ (e + p)\ u\ ]^T$. Where ρ is the density, p the pressure, u the velocity in x-direction and e the total energy of fluid per unit volume. For the inflow boundary condition, the flow through the rotary valve is assumed to undergo sudden contraction and abrupt expansion, the equation being solved by assuming the isentropic flow and estimating loss of stagnation pressure due to the abrupt expansion. Moreover, the flow field in front of and behind the rotary valve is assumed to be quasi-steady. For the outflow boundary condition, atmospheric conditions are imposed. The numerical fluxes for convective terms of Eq. (1) are evaluated by the TVD scheme (Yee, 1989), and are extended to third-order by MUSCL interpolation based on the primitive variables. Finally, using these values obtained by the interpolating method at cell interfaces, numerical fluxed are obtained by Roe's approximate Riemann solver. The three-stage Runge-Kutta method is used for the time integration.

The other computational domain corresponds to flow field downstream of the pipe end. Figure 2 shows schematic view of the computational domain. In the figure, r denotes radius of the pipe, or r = 6.5 mm. The two-dimensional axisymmetric Euler equation is applied to the flow field as the governing equation, which is represented by Eq. (2),

$$\frac{\partial \boldsymbol{U}}{\partial t} + \frac{\partial \boldsymbol{E}}{\partial x} + \frac{\partial \boldsymbol{F}}{\partial y} + \boldsymbol{H} = 0 \tag{2}$$

$$\boldsymbol{U} = \begin{bmatrix} \rho \\ \rho u \\ \rho v \\ e \end{bmatrix},\quad \boldsymbol{E} = \begin{bmatrix} \rho u \\ \rho u^2 + p \\ \rho uv \\ (e+p)u \end{bmatrix},\quad \boldsymbol{F} = \begin{bmatrix} \rho v \\ \rho uv \\ \rho v^2 + p \\ (e+p)v \end{bmatrix},\quad \boldsymbol{H} = \begin{bmatrix} \rho v \\ \rho uv \\ \rho v^2 \\ (e+p)v \end{bmatrix}$$

where v is the velocity in y-direction. Since sound pressure which is audible is 20 μPa to 20 Pa, which is about 10^{-4} times of magnitude lower than the flow pressure, highly accurate scheme is required to capture flow properties and noise. Hence we used fifth-order MUSCL-TVD scheme (Yamamoto, 1999) in evaluating unknown variables at cell interface. The process of evaluation of numerical fluxes is the same as that of one-dimensional flow except the MUSCL interpolation. The boundary conditions are indicated in Fig. 2, where the properties obtained by one-dimensional flow calculation are imposed on the inflow boundary. Regarding the outflow boundary condition, Thompson's nonreflecting boundary conditions (1987, 1990) are applied in order to prevent undesirable reflections generated there from influencing the flow properties. As for the time integration, three-stage Runge-Kutta scheme is applied.

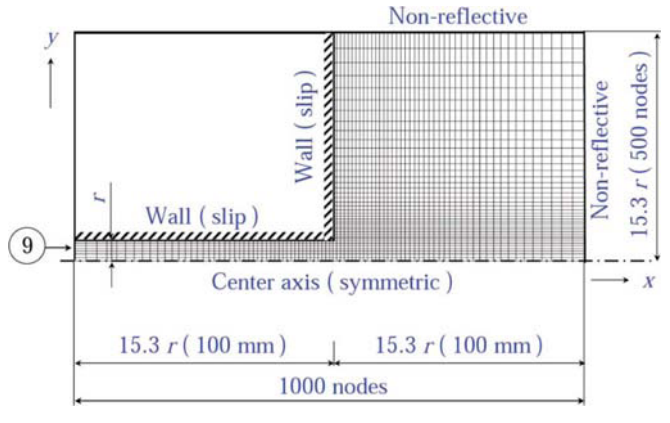

Fig. 2. Computational domain near the pipe end.

4. Results and Discussion

4.1 Pressure Histories in the Pipe

Figure 3 shows the pressure histories at each location along the pipe. The illustration shown in the left side of the figure shows the locations of pressure transducers. The opening area change of the rotary valve, which is normalized by cross-sectional area of the pipe, is shown by the curve at the bottom of the figure. The abscissa indicates time t normalized by a period of one cycle of rotary valve t. Time t is measured from the moment when the rotary valve opens and t = 10 msec. The ordinate is measured pressure, p, normalized by ambient pressure p_{atm}. The numbered lines in the figure show the traces of the head of first and second compression wave to be mentioned later. In the figure, compression wave generated by opening of the rotary valve propagates downstream with time, the gradient of the wave becoming steep as it propagates downstream. The compression wave is defined as first compression wave. Also, the expansion wave is produced after the moment when the opening area ratio of the rotary valve reaches its maximum, following the first compression wave. The expansion wave is reflected from the pipe end, which makes another compression wave propagating upstream. The wave generated by the reflection is defined as second compression wave. Observing the head of the first compression wave, the gradient may become steep as it propagates downstream. This phenomenon consists in the nonlinearity of compression wave in itself and the resultant generation of shock wave. Comparing the experimental result with the numerical one, the gradient of the head of first compression wave obtained by calculation is steeper than that by experiment. The difference can be explained by noting the governing Eq. (1) in which no frictional term appears.

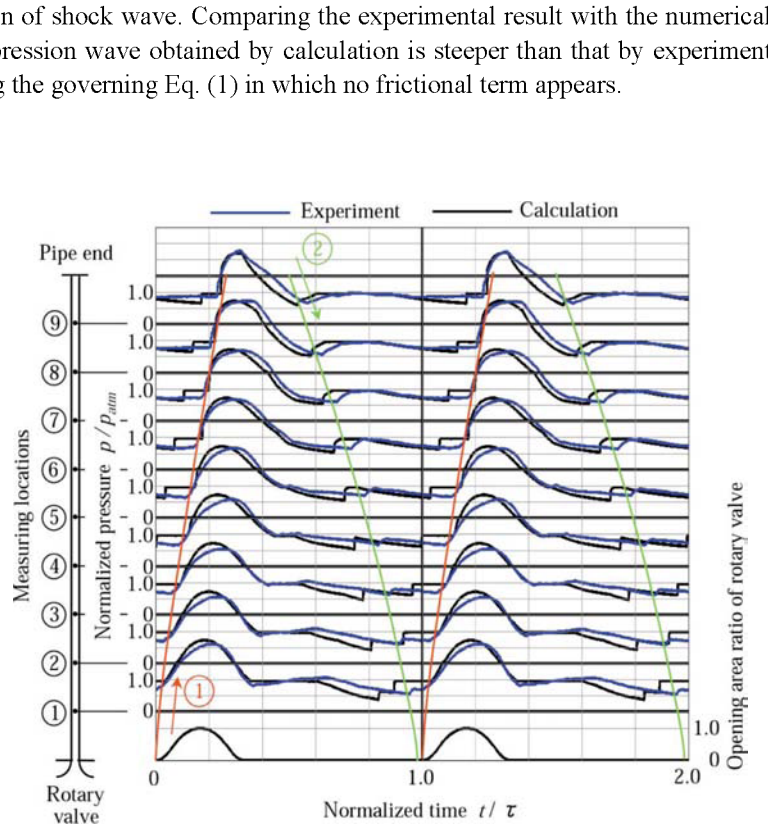

Fig. 3. Pressure histories in the pipe.

4.2 Visualization

Figure 4 shows schlieren and color schlieren photographs taken near the pipe end. t_d = 0.00 msec means the time when the shock wave generated and propagated downstream in the pipe stands exactly at the pipe end. In Figs. 4(a) and (d) the shock wave generated in the pipe is discharged, being diffracted spherically. The vortex ring also appears immediately after the moment when the shock wave is discharged. The subsonic jet, which is generated by opening of the rotary valve during the previous cycle, can be seen in front of the vortex ring. Three characteristic flow phenomena are obtained in Figs. 4(b) and (e). These are sound waves between the discharged shock wave and the vortex ring, the shock wave existing in the vortex ring and vortex ring streets in the shear layer of the underexpanded jet. The vortex ring streets can be identified by periodic change of the contrast in the schlieren

picture. It can be surmised that appearance of the sound waves is one of the causes of the noise generation in the pulsating jet. The mechanism of the noise generation is discussed in the next section. The formation of the shock wave imbedded in the vortex ring can be explained by the convergent-divergent nozzle effect (Minota, 1997). The passage of flow through the vortex ring interacts with the vortex sheet of the vortex ring. The shape of the vortex sheet plays a role of the throat of convergent-divergent nozzle. In Figs. 4(c) and (f) the cellular structure of the underexpanded jet develops as the stagnation pressure at the pipe end increases.

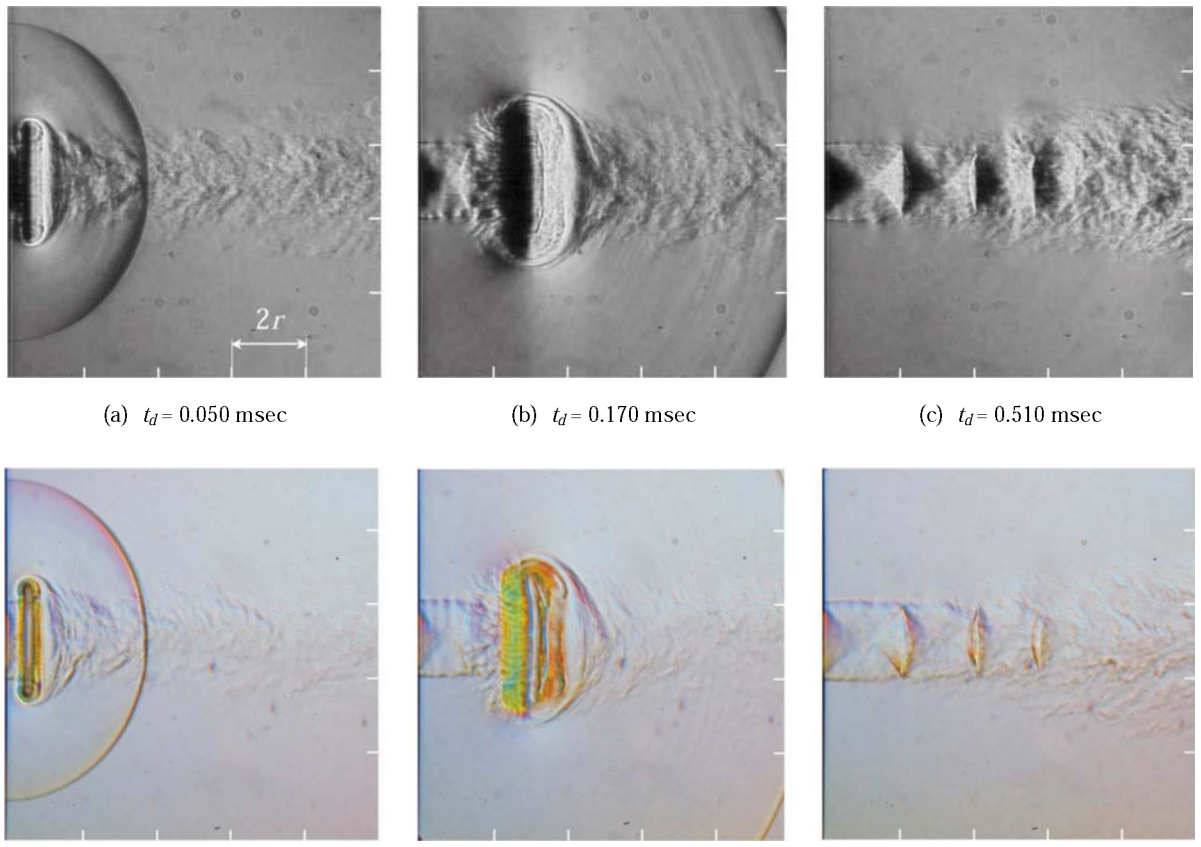

(a) t_d = 0.050 msec (b) t_d = 0.170 msec (c) t_d = 0.510 msec

(d) t_d = 0.050 msec (e) t_d = 0.170 msec (f) t_d = 0.510 msec

Fig. 4. Schlieren and color schlieren pictures.

4.3 Numerical Visualization

Comparison between experimental and numerical results of the flow field near the pipe end is examined before proceeding with the discussion of numerical visualization. Figure 5 shows the definition of various distances shown in Fig. 6. The X_s and X_v are distances from the pipe end to the discharged shock wave and the core of the main vortex ring, respectively. The X_u is the length of the first cell of the underexpanded jet. The Y_v is the radius of the main vortex ring. In Fig. 6, the comparison between experimental and numerical results is made. It is obvious that the flow fields agree with each other. However, it is found in Fig. 5 that the vortices along the slipstream are visible only in numerical shadowgraphy. The governing equation in the present study is Euler equation in which the numerical viscosity involved in the spatial discretization plays a substitute role of the physical viscosity, which may, as contrasted with experiments and turbulence modeling, produce a lot of vortices along the slipstream. Although it is impossible or very difficult to quantitatively estimate the vorticity and the frequency of the generation concerning the vortices due to the nature of the governing equation, it appears to be confirmed in Fig. 4(b) that the schlieren photograph which has higher sensitivity than shadowgraphy, especially with respect to small density variation, can capture at least the generation in itself. Therefore, the following discussion seems to be still valid from the qualitative viewpoint.

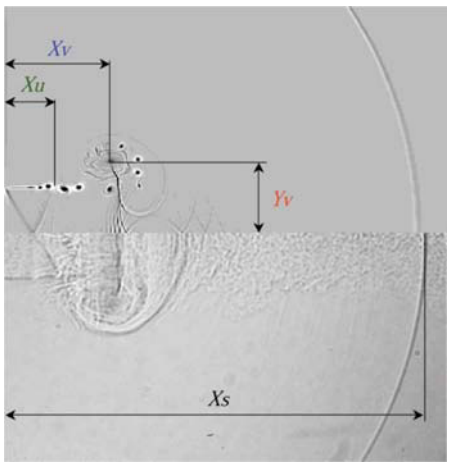

Fig. 5. Measuring distance (shadowgraphy); calculation: upper half, experiment: lower half.

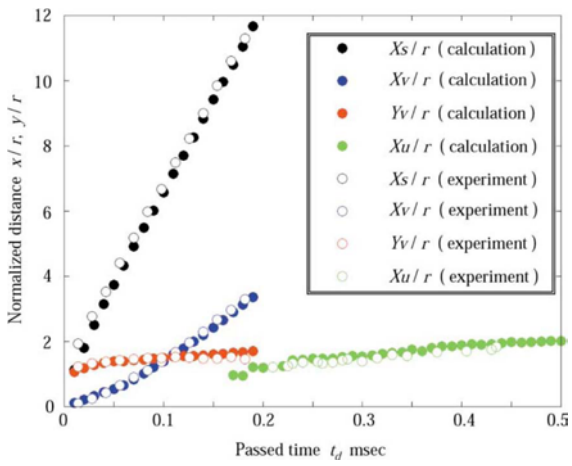

Fig. 6. Comparison between experimental and numerical results.

Figure 7 shows a series of computed schlieren pictures (just cross-sectional images), density contours and relative Mach number distributions on the jet axis. The velocity which is given by the difference between a local speed of jet on its axis and a convective velocity of a main vortex ring is divided by the local speed of sound on the jet axis, which is defined as relative Mach number, M_r. It should be noted from Fig. 6 (or Fig. 8) that the convective velocity of a main vortex ring keeps a constant value as it travels downstream. M_r is derived by using this feature. In Fig. 8, X_{vs} is the axial location of the shock wave in the vortex ring. X_{ch} and $X_{m\max}$ are the axial locations where M_r takes sonic speed and maximum value before and after the shock generation in the vortex ring, respectively. M_j is the jet Mach number estimated under assumption of the isentropic expansion of the stagnation pressure at the pipe end. The maximum values of M_r inside the vortex ring with t_d are denoted by $M_{r\max}$ in Fig. 8. It is found in Fig. 7(a) that as the development of the vortex sheet begins to narrow the passage of the following jet, this process and increment of M_j making M_r increase furthermore. In Fig. 7(b), M_r is accelerated to supersonic speed through the vortex ring, suddenly dropping to subsonic speed at the position of the shock wave being generated. At this time, inside of the vortex ring is fully covered with the shock wave. It appears from the distribution of M_r that flows passing through the vortex ring and the shock wave generation are very similar in flow pattern to those of a convergent-divergent nozzle mentioned above. The spherically propagating weak shock wave w_1 shown in Fig. 7(c) is produced by the interaction between the shock wave and the vortexlet v_1. Consequently, it can be easily expected that sound waves attenuated from weak shock waves in front of the vortex ring in Figs. 7(c) and (d) originate as a result of successive shock/vortex interaction, whereby the mechanism of the sound wave generation in Fig. 4(b) is also explainable.

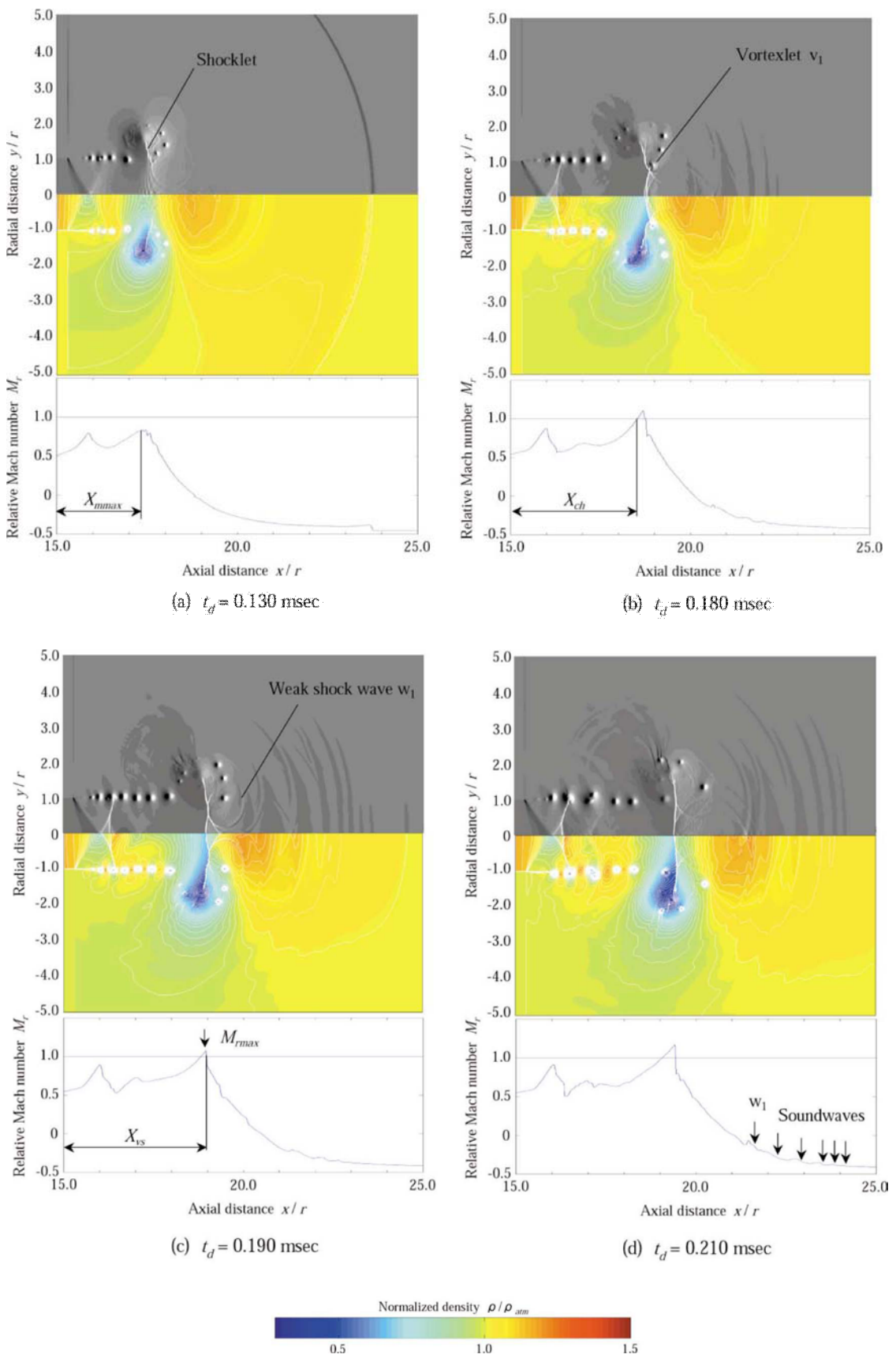

Fig. 7. Numerical visualization and relative Mach number distribution.

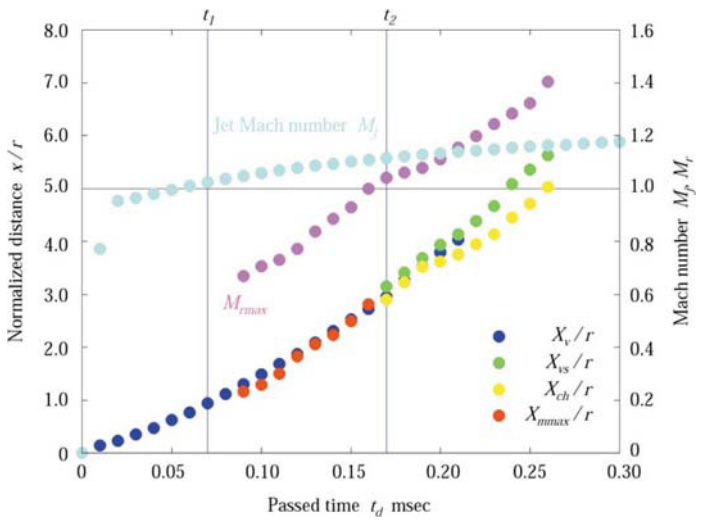

Fig. 8. Shock generation in vortex ring (t_1: start generating, t_2: fully generated).

Figure 9 shows computed schlieren photograph at t_d = 0.54 msec and M_j takes maximum value of 1.22 at this time. Needless to say, there are so many papers concerning the supersonic free jet and its sound emission. It is not easy to apply those results to the present study since these papers are concerned only with the jet steadily issuing out of a nozzle. However, they are applicable because the property of the underexpanded jet does not vary suddenly during its development, that is to say, the assumption of quasi-steady flow can be introduced. The noise seen in supersonic jet is related to large-scale turbulent vortices, which is generated when the organized vortices are convected away at supersonic velocity compared with the ambience. This is called Mach wave emission. In Fig. 9, the spacing between neighboring vortices becomes large as they flow downstream. This acceleration motion of vortices makes disturbance inherent in a supersonic flow and leads to Mach wave emission (Nakamura and Yamaguchi, 1999). Taking its directivity into account, the Mach wave may propagate in the direction with an angle of about 35° from the jet axis toward the downstream. This angle corresponds to Mach angle estimated by using M_j = 1.22. Although the Mach wave emission is not obviously visible in Figs. 4(c) and (f) in experiment, it is strongly suggested from the sound pressure histories (Fig. 10) that the noise following the discharged shock wave has the same directivity as those of present simulation; the sound waves and Mach wave shown in Figs. 7 and 9, respectively. Note that the former also has directivity toward the jet axis.

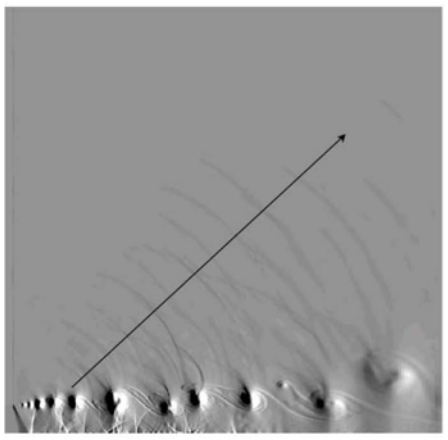

Fig. 9. Mach wave emission at t_d = 0.54 msec.

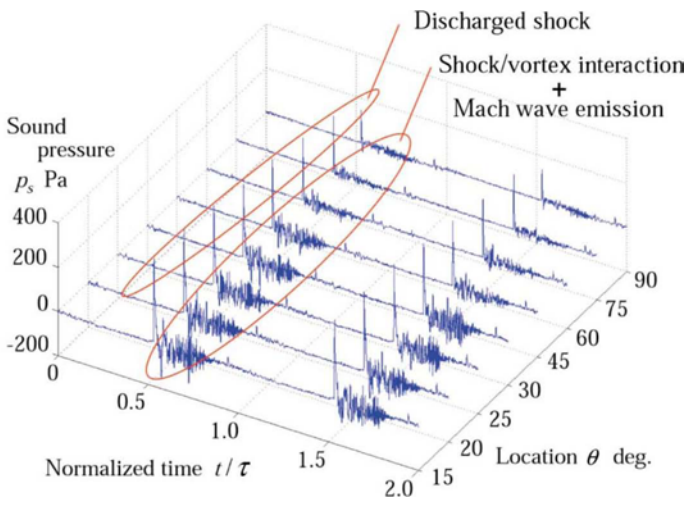

Fig. 10. Sound pressure histories.

5. Conclusion

In this study we experimentally and numerically studied the generation of noise seen in high-speed pulsating jet under the fixed condition of 6000 rpm of a real engine, and especially investigated the mechanism of noise generation from the numerical simulation. The results are summed up in the following:

1. The non-linearity of the compression wave propagating downstream through the pipe generates the shock wave, and the discharged shock wave from the pipe end becomes the primary noise source.
2. The interaction between the shock wave in the vortex ring and the vortexlets in the shear layer of the underexpanded jet makes sound waves directed downstream and towards the jet axis. This appears to be a characteristic of the pulsating jet.
3. The increment of the relative Mach number introduced in this study depends on the development of the vortex sheet of the vortex ring and the jet Mach number, and the shock wave in the vortex ring may generate in the same manner as that of a convergent-divergent nozzle when the relative Mach number across the vortex ring is accelerated to supersonic speed.
4. The appearance of the underexpanded jet leads to the Mach wave emission. It seems to be possible that the directivity is approximately expected by the jet Mach number estimated from the stagnation pressure at the pipe end under the assumption of isentropic expansion, which well agrees with the results of the sound pressure histories in the experiment.

References

Blair, G. P. and Goulburn, J. R., The Pressure-Time History in the Exhaust System of High-Speed Reciprocating Internal Combustion Engine, SAE Transactions, 670477 (1967).

Blair, G. P. and Arbuckle, J. A., Unsteady Flow in the Induction System of a Reciprocating Internal Combustion Engine, SAE paper, 700443 (1970).

Endo, M. and Iwamoto, J., A Study of Pulsatile Jet Discharged from Pipe End, Journal of Visualization, 1-3 (1999), 261-269.

Iwamoto, J., Experimental Investigation of a Rotary Valve, Research Reports of the Faculty of Engineering Tokyo Denki University, 22 (1974), 127-150.

Minota, T., Shock/Vortex Interaction in a Flow Field behind a Shock Wave Emitted from a Shock-Tube, Proceedings of 2nd International Workshop on Shock-Wave/Vortex Interaction (Sendai), (1997), 149-160, Shock Wave Research Center Institute of Fluid Science Tohoku University.

Nakamura, Y. and Yamaguchi, H., Compressible Jet and Its Sound Emission, Computational Fluid Dynamics Journal, 8-2 (1999), 250-256.

Thompson, K. W., Time Dependent Boundary Conditions for Hyperbolic Systems I, Journal of Computational Physics, 68 (1987), 1-24.

Thompson, K. W., Time Dependent Boundary Conditions for Hyperbolic Systems II, Journal of Computational Physics, 89 (1990), 439-461.

Yamamoto, S., Shock-Vortex Capturing Method and Its Application to Unsteady 3-D Cascade Flow, Computers & Fluids, 8-2 (1999), 341-349.

Yee, H. C., A Class of High-Resolution Explicit and Implicit Shock-Capturing Methods, NASA Technical Memorandum, 101088 (1989), 1-218.

Author Profile

Atsunori Kimura: He received his BSc (Eng) and MSc (Eng) degree in Mechanical Engineering from Tokyo Denki University in 1998 and 2000, respectively. Now he is in pursuit of his Ph.D. in the same university.

Junjiro Iwamoto: He received his BSc (Eng) and MSc (Eng) degree in Mechanical Engineering in 1962 and 1966, respectively from College of Engineering, Keio University, and his Ph.D. in High-Speed Oscillatory Flow in 1970 from Keio University. He worked as an engineer for Toyota Motor Company from 1962 to 1964. He took up his position as an assistant professor at Tokyo Denki University in 1969. In 1980 he was promoted to professor of mechanical engineering at Tokyo Denki University. His research interests include high-speed flow, shock dynamics and pulsating flow.